Atmos. Chem. Phys. Discuss., 9, 12141–12170, 2009
www.atmos-chem-phys-discuss.net/9/12141/2009/

Atmospheric Chemistry and Physics Discussions

This discussion paper is/has been under review for the journal *Atmospheric Chemistry and Physics (ACP)*. Please refer to the corresponding final paper in *ACP* if available.

Northern winter stratospheric temperature and ozone responses to ENSO inferred from an ensemble of Chemistry Climate Models

C. Cagnazzo[1], E. Manzini[1,2], N. Calvo[3], A. Douglass[4], H. Akiyoshi[5], S. Bekki[6], M. Chipperfield[7], M. Dameris[8], M. Deushi[9], A. Fischer[10,*], H. Garny[8], A. Gettelman[11], M. A. Giorgetta[12], D. Plummer[13], E. Rozanov[10,15], T. G. Shepherd[14], K. Shibata[9], A. Stenke[8], H. Struthers[16,], and W. Tian[7]**

[1]Centro Euro-Mediterraneo per i Cambiamenti Climatici, Bologna, Italy
[2]Istituto Nazionale di Geofisica e Vulcanologia, Bologna, Italy
[3]National Center for Atmospheric Research, Boulder, CO, USA
[4]NASA Goddard Space Flight Center, Greenbelt MD, USA
[5]National Institute for Environmental Studies, Tsukuba, Japan
[6]Service d'Aeronomie du CNRS, IPSL, Paris, France
[7]School of Earth and Environment, University of Leeds, Leeds, UK
[8]DLR-Institut für Physik der Atmosphäre, Oberpfaffenhofen, Germany

[9] Meteorological Research Institute, Tsukuba, Ibaraki 305-0052, Japan
[10] Institute for Atmospheric and Climate Science, ETH Zurich, Zurich, Switzerland
[11] National Center for Atmospheric Research, Boulder, CO, USA
[12] Max Planck Institute for Meteorology, Hamburg, Germany
[13] Environment Canada, Toronto, Ontario, Canada
[14] Department of Physics, University of Toronto, Toronto, Ontario, Canada
[15] Physical-Meteorological Observatory/World Radiation Center, Davos, Switzerland
[16] National Institute of Water & Atmospheric Research, Auckland, New Zealand
[*] now at: Federal Office of Meteorology and Climatology MeteoSwiss, Zurich, Switzerland
[**] now at: ITM – Stockholms universitet, Stockholms, Sweden

Received: 10 April 2009 – Accepted: 1 May 2009 – Published: 15 May 2009

Correspondence to: C. Cagnazzo (cagnazzo@bo.ingv.it)

Published by Copernicus Publications on behalf of the European Geosciences Union.

Abstract

The connection between the El Niño Southern Oscillation (ENSO) and the northern polar stratosphere has been established from observations and atmospheric modeling. Here a systematic inter-comparison of the sensitivity of the modeled stratosphere to ENSO in Chemistry Climate Models (CCMs) is reported. This work uses results from a number of the CCMs included in the 2006 ozone assessment. In the lower stratosphere, the mean of all model simulations reports a warming of the polar vortex during strong ENSO events in February–March, consistent with but smaller than the estimate from satellite observations and ERA40 reanalysis. This anomalous warming is associated with an anomalous dynamical increase of total ozone north of 70° N that is accompanied by coherent total ozone decrease in the Tropics, in agreement with that deduced from the NIWA total ozone database, implying an increased residual circulation in the mean of all model simulations, during ENSO. The spread in the model responses is partly due to the large internal stratospheric variability but it is shown that it crucially depends on the representation of the tropospheric ENSO teleconnection in the models.

1 Introduction

The El Niño Southern Oscillation (ENSO) is a tropical atmosphere-ocean phenomenon and a source of large-scale climate variability for the atmosphere-ocean system. During boreal winter, the typical teleconnection between the warm phases of ENSO and the mid-latitude North Pacific region (Hoerling et al., 1997; Strauss and Shukla 2000 among others) can favour the enhancement of mid-latitude planetary waves and consequently their upward propagation into the stratosphere. Due to this increase in extratropical stratospheric planetary wave activity, warm ENSO events have been found to be associated with anomalous warming and anomalously high geopotential height in the polar stratosphere, both from observations (van Loon and Labitzke, 1987; Hamil-

ACPD

9, 12141–12170, 2009

ton, 1993; Camp and Tung, 2007; and Garfinkel and Hartmann, 2007) and comprehensive modeling of the troposphere-stratosphere system (Sassi et al., 2004; Taguchi and Hartmann, 2006; Manzini et al., 2006; Garcia-Herrera et al., 2006). At high Northern latitudes, large zonal mean anomalies, in temperature and zonal wind, associated with the warm phase of ENSO appear in the upper stratosphere in early winter and then propagate downwards to the lower stratosphere on monthly time scale through wave mean flow interaction (Manzini et al., 2006). The modeling work of Manzini et al. (2006) has shown that these zonal mean anomalies associated with ENSO occur also in the troposphere in late winter and spring, and the subsequent modeling work of Cagnazzo and Manzini (2009) has shown that they are implicated in the surface teleconnection between ENSO and the North European region.

Given that the reported polar warming associated with warm ENSO events is a manifestation of an enhanced Brewer-Dobson circulation, more ozone should be transported from the source region in the tropics toward high polar latitudes during warm ENSO events. In fact, interannual variations in total ozone and temperature in the northern polar stratosphere are linked to planetary scale wave activity (Fusco and Salby, 1999; Randel et al., 2002; Weber et al., 2003). At Arctic and mid-latitude sites, an anomalous accumulation of total ozone was indeed reported for the strong and long lasting 1940–1942 ENSO event by Brönnimann et al. (2004). The response to ENSO has also been analysed in a few chemistry climate model (Fischer et al., 2008; Steinbrecht et al., 2006; Brönnimann et al., 2006) and in a chemical transport model (Sassi et al., 2004).

The purpose of this work is to extend these previous studies that analyzed the ENSO response in chemistry climate models (CCMs), by systematically evaluating the response to warm ENSO in the pool of simulations for the recent past performed with the CCMs participating to the Chemistry-Climate Model Validation Activity (CCMVal-1) of SPARC that are discussed in Eyring et al. (2006). Many of these models contributed to the last ozone assessment (WMO, 2007). These simulations have been performed with prescribed observed sea surface temperatures (SSTs), and therefore include the

ACPD
9, 12141–12170, 2009

ENSO forcing on the modeled atmosphere. However, the manifestation of the ENSO effect on the stratosphere depends also on the ENSO teleconnection in the troposphere, not necessary similarly represented in the CCMs. Another aspect obscuring the ENSO signal in the stratosphere is the typical high variability of the boreal winter stratosphere.

The focus of this work is on the Northern polar stratosphere temperature and ozone response during boreal winter, for the 1980–1999 period. Specifically, we aim at identifying any coherence in the temperature and ozone responses across the chemistry climate models. This in turn may provide some insight into understanding the causes of the range of responses, in terms of simulation designs and model biases.

Note that the cold ENSO events that occurred in the 1980–1999 period have been found to have negligible influence on the Northern polar stratosphere during winter (Manzini et al., 2006; see also Sassi et al. 2004), and therefore are not considered in this work. The negligible response may be in partly due to the smaller SSTs anomalies occurred for cold events during the period considered here.

2 Datasets and methodology

2.1 Models

The CCM datasets used in this work result from transient runs aimed at reproducing the time period of 1980–1999 (Eyring et al., 2006): the simulations include anthropogenic and natural forcings based on changes in SSTs, trace gases, solar variability, and aerosol effects (from major volcanic eruptions). The models are summarized and referenced in Table 1. Modeled monthly zonal mean temperature and total ozone and (when available) monthly three-dimensional geopotential height fields have been analyzed. AMTRAC, CCSRNIES, MRI, SOCOL and WACCM models have provided a set of 3, 3, 5, 9 and 3 realizations (i.e., they have repeated the simulation of the 1980–1999 period with different meteorological initial conditions), respectively. SOCOL, E39C-A

ACPD
9, 12141–12170, 2009

and MRI models have provided outputs from updated model versions with respect to those described in Eyring et al. (2006). The analysis on the AMTRAC, GEOSCCM, and 2 members of CCSRNIES simulations is restricted to the zonal mean fields, because three-dimensional fields were not available for these cases.

2.2 Observations and reanalysis data

Three datasets covering the 1980–1999 period, are considered:

1. Time series of monthly mean temperature and geopotential height from the European Centre for Medium-Range Weather Forecast Re-Analysis (ERA-40, Uppala et al., 2004).
2. Stratospheric Sounding Unit (SSU) temperatures (Nash and Edge, 1989; Brindley et al., 1999) and Microwave Sounding Unit (MSU) temperatures (Spencer and Christy, 1995). These datasets consist of zonal temperature anomalies every 10 degrees from 70° S to 70° N for the 3 SSU channels (anomalies peaking at 15, 6, and 2 hPa) and 4 synthetic channels (peaking at 50, 20, 5, 1.5 and 0.5 hPa, Nash and Edge, 1989) and for the MSU channel (90 hPa).
3. NIWA total ozone dataset, which combines data from several United States and European satellites with a global set of ground stations (Bodecker et al., 2005).

2.3 Diagnostics

Composites for the period 1980–1999 are constructed for temperature, total ozone and eddy geopotential heights fields. For each month of the extended winter season (October to April), warm ENSO and NEUTRAL composites of monthly means are considered, for the models and the datasets. Our standard warm ENSO composite is made up of the 4 largest warm events that occurred in the period 1980–1999 (hereafter 4 WE), see Table 2 for the list of the events. The events are selected on the basis of the SST anomaly averaged from January to March in the Nino-3 region from the National Centers for Environmental Prediction (NCEP)/Climate Prediction Center

ACPD
9, 12141–12170, 2009

(CPC) (http://www.cpc.ncep.noaa.gov/data/indices). These four events are those typically studied in climate research on ENSO teleconnections, for example Strauss and Shukla (2000) and Manzini et al. (2006). Following Manzini et al. (2006), the NEUTRAL composite is made of the years within the 1980–1999 period, that exclude these warm ENSO events as well as the 4 largest cold ENSO events (see Table 2). Two of the four winters considered in the warm ENSO composite analysis were disturbed by volcanic eruptions (1982–1983 and 1991–1992). Intense volcanic eruptions cause a cooling and a strengthening of the vortex (Labitzke and Van Loon, 1989) possibly leading to a distortion of the anomaly associated with ENSO in the polar stratosphere. For this reason, a second warm ENSO composite has been constructed, including two additional ENSO events (hereafter 6 WE, see Table 2), with the two additional events not disturbed by the volcanic external forcing, albeit characterized by weaker ENSO phenomena. In this analysis, no distinction between models including or not the QBO or the solar cycle is performed.

For every field considered, "ENSO anomalies" are defined as the difference between the warm ENSO composite and the NEUTRAL composite.

In order to compactly compare the response of each model to the ENSO forcing, the following 4 indices are defined and calculated from the ENSO anomalies:

ΔT *index*, defined as the February–March, polar cap (70° N–90° N) and 30–70 hPa average of the ENSO zonal mean temperature anomaly (<T>ENSO–<T>NEUTRAL). This index represents the temperature anomaly associated to ENSO in the lower stratosphere at the end of winter/beginning of spring.

ΔZ *index*. The known tropospheric teleconnection of ENSO with Northern midlatitude stationary waves in December–January–February (DJF) consists of an eastward elongation of the North Pacific trough (Hoerling et al., 1997). In order to quantify this typical tropospheric pattern, we defined the ΔZ index in the following way: At 50° N and 500 hPa, for the DJF average: (1) The difference between the warm ENSO and the neutral ENSO composites, of the stationary eddy geopotential height is computed and defined to be the tropospheric stationary wave anomaly. (2) The minimum value of

ACPD
9, 12141–12170, 2009

the tropospheric stationary wave anomaly between 180 and 360 longitude is searched and found. (3) This minimum value is smoothed by an average over 10% of its value. (4) The absolute value of the smoothed minimum of the tropospheric stationary wave anomaly is the ΔZ index. Therefore, the ΔZ index is always positive.

ΔO3 index, defined as the February–March, polar cap (70° N–90° N) average of the ENSO zonal mean total ozone anomaly (<O3>ENSO–<O3>NEUTRAL). This index is aimed at quantifying the total ozone anomaly associated to the ENSO teleconnection in February and March in the polar region only.

ΔO3 (FM-ND) index, defined as the February–March mean minus the November–December mean of an area average of the ENSO zonal mean total ozone anomaly. This index has been calculated for the polar cap (70° N–90° N) and the tropics (15° S–15° N) ((<O3(FM)>–<O3(ND)>)ENSO–(<O3(FM)>–<O3(ND)>)NEUTRAL) and it represents the wintertime increase/decrease in the ENSO zonal mean total ozone anomaly at polar/tropical latitudes. Salby and Callaghan (2002) have shown that it is the tendency (i.e. the anomalous wintertime increase of total ozone at high latitudes) that is coupled to the residual circulation, not the ozone directly. Fusco and Salby (1999) and Hadjinicolaou et al. (1997) found that the change of ozone during one year is directly related to the ozone change during the same year not to an accumulation from previous years. Therefore, it interesting to analyze this tendency in order to quantify the ozone changes due to the dynamical variability associated with ENSO.

3 Temperature in the lower stratosphere

Figure 1 shows the time evolution from October to April of the ENSO zonal mean temperature anomalies at 70° N, from 100 hPa to 0.1 hPa, for the composite of the 4 warm events (top) and the 6 warm events (bottom), for both the SSU/MSU (left) and ERA40 (right) data. Figure 1 shows that in the case of the 4 largest ENSO events, the polar warming occurs first in the upper stratosphere (about 4 K for SSU and 8 K for ERA40, significant in December at 95%) and then descends to the lower stratosphere (about

ACPD
9, 12141–12170, 2009

4 K between 50 and 100 hPa significant in January and February at 90% for SSU/MSU, and reaching 95% for ERA40). In the upper stratosphere, the cooling above the warming may be a manifestation of a large-scale dynamical response involving the circulation in the mesosphere. Figure 1 also shows that the warming associated to ENSO is reduced when considering the 6 largest ENSO events (4 K between 10 and 1 hPa; 2 K in the lower stratosphere for SSU/MSU; 6 K between 10 and 1 hPa; 2 K in the lower stratosphere for ERA40; the signal is significant at 95% in the upper stratosphere and not significant in the lower stratosphere for both the datasets). This result is consistent with the fact that ENSO is weaker for the two additional cases. Therefore, the response is reduced and less significant due to the internal variability of the Northern polar stratosphere. Figure 1 also shows that the temperature response at 70° N in December, January and February is the same for ERA40 and SSU/MSU below 20 hPa, but it is about the double for ERA40 above. These results are in agreement with observational studies, in particular with Camp and Tung (2007) who applied a linear discriminant analysis on 47 years of NCEP stratospheric temperature (10–50 hPa) and found that the warm-ENSO years are 4 K significantly warmer. In the upper stratosphere the ENSO anomalies derived from the ERA-40 data have also been found to be larger than those derived from the NCEP/CPC (Manzini et al 2006). In our analysis we will focus on the region between 30 hPa and 70 hPa.

Because we are interested in changes that might be relevant for ozone, we compact the reporting of the model response to ENSO, by plotting the time evolution from October to April of the zonal mean temperature response to ENSO in the lower stratosphere (30–70 hPa) over the polar cap (70° N–90° N) as shown in Fig. 2. The results from ERA40 and SSU shown in Fig. 2 reproduce those deduced from Fig. 1. In Fig. 2 (left), one curve per model is plotted, i.e. the anomaly has been averaged over the set of multiple realizations performed by the same model, when available, in order to better compact the results. In the right panels of Fig. 2 we estimate the response to ENSO, by computing the mean of all simulations and its significance, the latter estimated with a t-Student test performed over the total number (30) of available simulations.

ACPD
9, 12141–12170, 2009

For the 4WE anomaly (Fig. 2 top-right), the largest temperature warming is obtained in February (about 7 K for ERA40 and 5.5 K in SSU), whereas for the mean of all model simulations the largest warming is found in March (2.8 K, significant at 95%). The mean of all model simulations is positive and significant in February (2 K, significant at 90%) and in April (1.8 K, significant at 90%). The warming for the mean of all model simulations in late winter and spring is relatively small compared with the reanalysis and satellite data, because the models show quite variable responses (see the spread of the colored curves on Fig. 2, left). For some models, the largest positive anomaly at these altitudes is found in January or even in March–April; for three of them the positive anomaly is greater than SSU, but lower than ERA40; and three models do not show any warming in this layer. Bearing in mind the internal stratospheric variability, we can conclude that the ERA40, SSU and the model results are qualitatively consistent. Associated with this stratospheric warming, a weakening of the polar vortex is found, that is highly variable across the models (not shown).

The analysis of Figs. 1 and 2 shows that the time evolution of the temperature anomaly for the 6 warm ENSO events, with the two additional events not disturbed by the volcanic external forcing, is similar but slightly weaker than the anomaly for the 4 largest ENSO events for the model mean. From here on the analysis will focus on the 4 warm ENSO composite only.

4 Troposphere teleconnection and link to the response in the stratosphere

In order to relate the modeled response in the polar lower stratosphere to the representation of the ENSO teleconnections with the troposphere (specifically, with the mid-latitude North Pacific region), the relationship between the ΔZ index (see Sect. 2), measure of the ENSO tropospheric teleconnection, and the ΔT index, measure of February–March polar lower stratosphere temperature anomaly, is shown in Fig. 3 (the ΔZ index has been calculated for 24 of the 30 simulations).

ACPD
9, 12141–12170, 2009

The ΔT index distribution across the simulations tends to be positive (Fig. 3, top-left): 18 simulations show positive response, 6 simulations a negative response, with the largest occurrence in the positive anomaly associated to the 2–3 K bin. These results summarize Fig. 2. The distribution of the ΔZ index across the simulations (shown in Fig. 3 bottom-right) indicates that the response is variable also for this index. This index is a quantitative estimate of the tropospheric stationary wave anomaly during strong ENSO episodes. Consequently, a large value of this index can imply an increase of vertically propagating planetary waves emerging from the troposphere. The maximum occurrence for this index for the model data pool is found in the 40–55 m bin, whereas the ΔZ index for ERA40 is higher (103 m). The index for ERA40 is about twice its standard deviation. This implies that the ENSO extratropical response in the eddy geopotential height field is quite robust. This result shows that the ENSO tropospheric stationary wave anomalies are stronger for ERA40 than for the majority of the simulations (note that ERA40 is dominated by the large 1998 ENSO event, not shown). A positive correlation (0.31, significant at 86%) between the temperature in the lower stratosphere and the tropospheric stationary wave anomaly is found (Fig. 3, top-right). This behavior indicates that when the tropospheric response to ENSO in the North Pacific region is large, the response in the lower stratosphere in temperature during spring is also large. Simulations with the lowest ΔZ index (i.e., lower than 40 m) report a negative temperature anomaly during ENSO. Visual inspection of the individual modeled anomalies (not shown) has revealed that at least some of these models may anyway have a polar stratospheric warming, but either confined above 30 hPa or occurring in a different time (January or April). An important result of Fig. 3 is that differences among the simulations in the ΔZ index are almost twice larger than the differences within the multiple realization runs of a model (see the ΔZ index range for WACCM, MRI, and SOCOL). An explanation of this result is that the tropospheric ENSO teleconnection is substantially different among the models. Therefore, the spread in this index among the simulations is related to both differences in model formulations and variability of the ENSO extra-tropical tropospheric teleconnections. On the other hand, the spread

ACPD
9, 12141–12170, 2009

in the ΔT index for each of the ensemble simulations is indicative of the stratospheric internal variability, and suggests that even with a similar ENSO teleconnection in the troposphere (see for example WACCM), there is variability in the lower stratospheric response (from negative to positive).

5 Ozone

The impact of ENSO on the total ozone distribution is illustrated in Fig. 4 for the models, the NIWA dataset and for the mean of all model simulations, at polar latitudes (70° N–90° N average, top) and in the Tropics (15° S–15° N average, bottom).

In the polar region, the NIWA total ozone anomaly is negative from October to January and positive in February, March and April. The NIWA total ozone positive anomaly is largest in February (~20 DU). The model responses show a large spread, especially in January, February and March. The total ozone anomaly in the mean of all model simulations is positive from January to April and reaches ~10 DU in March (not significant). In the tropical regions (Fig. 4, bottom), negative ozone anomalies are observed throughout the whole winter season. The largest negative anomalies are again obtained for the same months: in February (−7 DU) for NIWA and in March (−6 DU, significant at 95%) for the mean of all model simulations. Figure 4 demonstrate that for the ENSO anomalies, an increase of the total ozone in the Arctic (top) is accompanied by a coherent total ozone decrease at tropical latitudes (bottom).

The accumulation of ozone at high latitudes is indicative of stronger diabatic descent during ENSO in that region, consistent with a warmer polar lower stratosphere (Fig. 2) and an increased Brewer Dobson circulation. The total ozone decrease in the tropics is consistent with increased ascent in the lower stratosphere circulation and, again, increased Brewer-Dobson circulation). More than for the temperature, the total ozone anomaly across the models at high latitudes is highly variable showing a large spread in the model responses. On the other hand, in the tropics the response across the models is consistent and quite robust (Fig. 4, bottom-left and the significance in the bottom-

ACPD
9, 12141–12170, 2009

right). Note however that in the tropics the total ozone is also directly affected by ENSO, because during ENSO the warmer sea surface temperatures lead to a warmer troposphere and a higher tropopause throughout most of the tropics. The higher tropopause in turn implies a decrease of the tropical column ozone (Shiotani, 1992; Steinbrecth et al., 2006). The response in the tropical lower stratosphere can also be directly related to local tropical wave forcing (Deckert and Dameris, 2008; McLandress and Shepherd, 2008), a topic not addressed in the current work.

In order to evaluate if a quantitative relationship exists between the modeled ENSO anomalies in lower stratospheric temperature and in total ozone, Figure 5 reports a scatter plot of the ΔO3 index versus the ΔT index (see Sect. 2). A clear positive correlation (0.85, significant at more than 99.9%) between the modeled total ozone and temperature anomalies is found. The relationship between the ERA40 temperature and the NIWA total ozone is located very close to the regression line, providing evidence for the physical consistency of the relationship found by the model results during ENSO. Moreover, Fig. 5 shows that the positive correlation appears also for the 9 realizations from the SOCOL model and possibly the 5 realizations from the MRI model, and that spread among the models is comparable to the spread among the same-model realizations of either SOCOL or MRI. These results indicate that the non-linearity of the system appears to play a dominate role, possibly obscuring differences due to model formulation and that whilst the internal variability in the lower stratosphere during winter/spring can be large, the relationship between ozone and temperature anomalies is robust.

In order to identify the ozone accumulation controlled by dynamical variability during ENSO in the lower stratosphere, we examine the anomalous wintertime ozone tendency. The anomalous wintertime increase of total ozone at high latitudes and decrease at low latitudes is defined as the anomalous tendency of total ozone from the beginning of winter to the end of winter/beginning of spring and is analyzed following Salby and Callaghan (2002) and Fusco and Salby (1999). Figure 6 (left) shows the distribution of the ΔO3(FM-ND) index (Sect. 2) at polar (top) and tropical (bottom) lati-

ACPD
9, 12141–12170, 2009

tudes. The dynamical total ozone accumulation to the tropospheric ENSO response of each model is evaluated by plotting the relationship between the ΔO3(FM-ND) index and the ΔZ index is also shown in Fig. 6 (right). The distribution of the ΔO3(FM-ND) index is clearly negative at tropical latitudes (with 23 simulations reporting a negative index and just one realization with a positive index) whilst it is generally positive (17 models) at high latitudes. In this case, the anomalous wintertime increase of total ozone at high latitudes represents the total ozone dynamical accumulation (i.e. ozone that is transported by anomalous residual circulation) with a negligible contribution of the dynamically-induced chemical effect (i.e. changes in ozone due to changes in photochemistry induced by dynamical changes in temperature), because ENSO years are anomalously warm.

Figure 6 (right) shows linear relationships between the wintertime dynamical ozone accumulation during ENSO (the ΔO3(FM-ND) index) and the ΔZ index, with a positive correlation (0.37, significant at 92%) at high latitudes and a negative one at tropical latitudes. This means that if the ΔZ index of a model is large, i.e. there is a strong teleconnection between ENSO and the North Pacific region, the model simulates more dynamically accumulated ozone during ENSO at polar latitudes and a decrease at low latitudes, reflecting enhanced stratospheric transport.

6 Summary and conclusions

A systematic CCM inter-comparison of the stratospheric temperature and ozone response to ENSO for the Northern winter is reported. Considered are model simulations made for the CCMVal-1 activity (presented and discussed in Eyring et al., 2006), of which many contributed to the last ozone assessment (WMO, 2007). The main results are summarized here:

1. In the lower stratosphere, the mean of all model simulations reports a warming of the polar vortex during strong ENSO events: the February–March temperature anomaly in the lower stratosphere is positive, significant and of the order of 2 K for

ACPD
9, 12141–12170, 2009

the mean of all model simulations. The response to ENSO obtained from the individual simulations is however highly variable, because of the large internal atmospheric variability and possibly also because of differences in model formulations. The mean anomaly derived from the model simulations is consistent with but smaller than the estimate from the SSU temperature (~4 K) and from ERA40 (~6 K) in the lower stratosphere.

2. The warming found in the mean of all model simulations in the polar lower stratosphere is associated with an increase of total ozone north of 70° N: the total ozone ENSO anomaly in the mean of all model simulations is positive and of the order of 10 DU in March. The dynamical increase of the total ozone in the Arctic during ENSO is accompanied by coherent total ozone decrease in the Tropics (−7 DU). The modelled anomalies are in very good agreement with those derived by the NIWA total ozone in the Tropics and consistent but about one half of the anomalies found with NIWA in the Arctic (~20 DU in February).

3. A novel result of this analysis is the positive correlation found between the ΔT index and the ΔZ index. The ΔZ index represents a measure of the eastward elongation of the north-west Pacific trough during warm ENSO years. As discussed in Manzini et al. (2006), this structure is persistent in time and may enhance the tropospheric forcing of upward propagating planetary wave one. Once the planetary wave one is enhanced also in the stratosphere, it can affect the zonal mean flow (by wave-mean flow interaction) and give rise to large-scale effects. Consistently, increased upward planetary wave propagation and convergence of the Eliassen-Palm flux has been found by Garcia-Herrera et al. (2006) for warm ENSO events. The positive correlation here found between the ΔT index and the ΔZ index reveals that the temperature response in the lower stratosphere depends on the representation of the tropospheric ENSO teleconnection: Simulations with large tropospheric stationary eddy anomaly in the eastern North Pacific region also report a large temperature response in the lower stratosphere during spring. The positive correlation found between the ΔO3(FM-ND) ozone accumulation index and the ΔZ index, significant at 92%, also corroborates the

ACPD
9, 12141–12170, 2009

dependence of the lower stratospheric response on the tropospheric ENSO teleconnection. The correlation between the ΔO3(FM-ND) index and the ΔZ index shows that simulations with a higher ΔZ index also report a larger ozone dynamical accumulation in the polar latitudes (and a decrease at tropical latitudes), consistent with increased circulation in the stratosphere. From the pool of CCM simulations considered, the relationship between the ΔO3(FM-ND) index and the ΔZ index indicates a sensitivity of the ozone accumulation of about 2.5 DU/(10 m).

4. The role of internal variability in the polar stratospheric ENSO response can be deduced by the spread in the temperature and ozone ENSO anomalies for the models that provided more than one realization of the 20-year period considered. We have found that the spread of the ΔZ index among the models tends to be larger than the spread within the realizations obtained by one model (MRI, SOCOL, WACCM). In particular, for the SOCOL model, for which there are 9 realizations, the spread between its realizations is about half the total spread. We also notice that a few models reports a ΔZ index below the standard deviation (50 m) of the stationary eddies of ERA40, suggesting that the tropospheric ENSO teleconnection for these models could be underestimated because of too little tropospheric variability. These results imply that tropospheric variability and differences in representing ENSO teleconnection in the troposphere, due to differences in model formulations, play a substantial role in the stratospheric response to ENSO.

To summarize, our systematic intercomparison of the sensitivity of the response to ENSO in the stratosphere for CCMs included in the CCMVal-1 activity is in agreement with previous analysis based on observational datasets (Brönnimann, 2004) and the SOCOL CCM (e.g. Fischer et al., 2008; Brönnimann et al., 2006). Namely, also the mean of all simulations from the pool of models considered here display a polar warming and an increased total ozone during ENSO years. Differently from the mentioned works in this analysis the ENSO signal in the lower stratosphere is considered to be non linear (following Manzini et al., 2006; Hoerling, 1997).

ACPD
9, 12141–12170, 2009

The reported modelled and observed warming in FM lower stratosphere and increase (decrease) in total column ozone at high (low) latitudes, is consistent with increased residual circulation during ENSO. Given the spread in the temperature and the ozone responses to ENSO, within the pool of available simulations, the strength of this increase is presumably also highly variable. The positive correlation (significant at more than 99%) found between the ENSO anomaly in temperature and total ozone indicates that the residual circulation is the main driver for the ΔT, ΔO3 covariance in response to ENSO.

The responses in the lower stratospheric temperature and in total ozone are highly variable indicating that the large internal stratospheric variability plays a major role in determining these responses. Nevertheless, by quantifying the tropospheric stationary eddy enhancement during ENSO and its variability across the model simulations, we have shown that the tropospheric ENSO teleconnections are important in explaining the range of responses in the lower stratospheric temperature and in total ozone. In fact, the new result concerning the correlations between the ΔZ index and the temperature and/or ozone indices suggest a strong link between the dynamical ENSO external forcing of the stratosphere and the strength of the response in the stratosphere and at least a part of the spread of the stratospheric responses across all the models comes from the spread in the midlatitude tropospheric response. This result is therefore the most promising for being used to differentiate between the role of internal variability and model formulation in a larger pool of realizations and models and it highlights that (tropospheric) modelling is important when attempting to accurately simulate the stratospheric response to ENSO forcing in Chemistry Climate Models.

Acknowledgements. Chiara Cagnazzo is supported by the Centro Euro-Mediterraneo per i Cambiamenti Climatici. Elisa Manzini acknowledges the support of the EC SCOUT-O3 Integrated Project (505390-GOCE-CT-2004) for part of this work. Natalia Calvo has been supported by the Spanish Ministry of Education and Science and the Fulbright Commission in Spain. CCSRNIES's research has been supported by the Global Environmental Research Fund (GERF) of the Ministry of the Environment (MOE) of Japan (A-071). MRI simulations have been made partly with the MRI supercomputer and partly with the NIES supercomputer.

We acknowledge the modeling groups for making their simulations available for this analysis, the Chemistry-Climate Model Validation Activity (CCMVal) for WCRP's (World Climate Research Programme) SPARC (Stratospheric Processes and their Role in Climate) project for organizing and coordinating the model data analysis activity, and the British Atmospheric Data Center (BADC) for collecting and archiving the CCMVal model output. Chiara Cagnazzo and Elisa Manzini are grateful to Antonio Navarra for useful discussions. We are thankful to John Austin for suggestions and discussions on the manuscript.

References

Akiyoshi, H., Zhou, L. B., Yamashita, Y., Sakamoto, K., Yoshiki, M., Nagashima, T., Takahashi, M., Kurokawa, J., Takigawa, M., and Imamura, T.: A CCM simulation of the breakup of the Antarctic polar vortex in the years 1980–2004 under the CCMVal scenarios, J. Geophys. Res., 114, D03103, doi:10.1029/2007JD009261, 2008.

Akiyoshi, H., Sugita, T., Kanzawa, H., and Kawamoto, N.: Ozone perturbations in the Arctic summer lower stratosphere as a reflection of NO_x chemistry and planetary scale wave activity, J. Geophys. Res., 109, D03304, doi:10.1029/2003JD003632, 2004.

Austin, J.: A three-dimensional coupled chemistry-climate model simulation of past stratospheric trends, J. Atmos. Sci., 59, 218–232, 2002.

Austin, J. and Butchart, N.: Coupled chemistry-climate model simulation for the period 1980 to 2020: Ozone depletion and the start of ozone recovery, Q. J. Roy. Meteor. Soc., 129, 3225–3249, 2003.

Austin, J. and Wilson, R. J.: Ensemble simulations of the decline and recovery of stratospheric ozone, J. Geophys. Res., 111, D16314, doi:10.1029/2005JD006907, 2006.

Austin, J., Wilson, R. J., Li, F., and Voemel, H.: Evolution of water vapor concentrations and stratospheric age of air in coupled chemistry-climate model simulations, J. Atmos. Sci., 64(3), 905–921, 2006.

Beagley, S. R., de Grandpre', J., Koshyk, J. N., McFarlane, N. A., and Shepherd, T. G.: Radiative-dynamical climatology of the first-generation Canadian Middle Atmosphere Model, Atmos. Ocean, 35, 293–331, 1997.

Bloom, S., da Silva, A., Dee, D., et al.: Documentation and validation of the Goddard Earth Observing System (GEOS) data assimilation system – Version 4, in Global Modeling Data Assimilation 104606, Tech. Rep. Ser. 26, NASA Goddard Space Flight Cent., Md., 2005.

Bodeker, G. E., Shiona, H., and Eskes, H.: Indicators of Antarctic ozone depletion, Atmos. Chem. Phys., 5, 2603–2615, 2005, http://www.atmos-chem-phys.net/5/2603/2005/.

Brindley, H. E., Geer, A. J., and Harries, J. E.: Climate variability and trend in SSU radiances: a comparison of model predictions and satellite observations in the middle stratosphere, J. Climate, 12, 3197–321, 1999.

Brönnimann, S., Luterbacher, J., Staehelin, J., Svendby, T. M., Hansen, G., and Svenøe, T.: Extreme climate of the global troposphere and stratosphere 1940–1942 related to El Nino, Nature, 431, 971–974, 2004.

Brönnimann, S., Schraner, M., Müller, B., Fischer, A., Brunner, D., Rozanov, E., and Egorova, T.: The 1986-1989 ENSO cycle in a chemical climate model, Atmos. Chem. Phys., 6, 4669–4685, 2006, http://www.atmos-chem-phys.net/6/4669/2006/.

Cagnazzo, C. and Manzini, E.: Impact of the stratosphere on the winter tropospheric teleconnections between ENSO and the North Atlantic and European Region, J. Climate, 22(5), 1223–1238, 2009.

Camp, C. D. and Tung, K.-K.: Stratospheric polar warming by ENSO in winter: A statistical study, Geophys. Res. Lett., 34, L04809, doi:10.1029/2006GL028521, 2007.

Dameris, M., Grewe, V., Ponater, M., Deckert, R., Eyring, V., Mager, F., Matthes, S., Schnadt, C., Stenke, A., Steil, B., Brühl, C., and Giorgetta, M. A.: Long-term changes and variability in a transient simulation with a chemistry-climate model employing realistic forcing, Atmos. Chem. Phys., 5, 2121–2145, 2005, http://www.atmos-chem-phys.net/5/2121/2005/.

Dameris, M., Matthes, S., Deckert, R., Grewe, V., and Ponater, M.: Solar cycle effect delays onset of ozone recovery, Geophys. Res. Lett., 33, L03806, doi:10.1029/2005GL024741, 2006.

de Grandpre', J., Beagley, S. R., Fomichev, V. I., Griffioen, E., McConnell, J. C., Medvedev, A. S., and Shepherd, T. G.: Ozone climatology using interactive chemistry: Results from the Canadian Middle Atmosphere Model, J. Geophys. Res., 105, 26 475–26 492, 2000.

Deckert, R. and Dameris, M.: Higher tropical SSTs strengthen the tropical upwelling via deep convection, Geophys. Res. Lett., 35, L10813, doi:10.1029/2008GL033719, 2008.

Egorova, T., Rozanov, E., Zubov, V., Manzini, E., Schmutz, W., and Peter, T.: Chemistry-climate model SOCOL: a validation of the present-day climatology, Atmos. Chem. Phys., 5, 1557–1576, 2005, http://www.atmos-chem-phys.net/5/1557/2005/.

Eyring, V., Butchart, N., Waugh, D. W., et al.: Assessment of temperature, trace species, and ozone in chemistry-climate model simulations of the recent past. J. Geophys. Res., 111, D22308, doi:10.1029/2006JD007327, 2006.

Fischer, A. M., Shindell, D. T., Winter, B., Bourqui, M. S., Faluvegi, G., Rozanov, E., Schraner, M., and Brönnimann, S.: Stratospheric winter climate response to ENSO in three chemistry-climate models, Geophys. Res. Lett., 35, L13819, doi:10.1029/2008GL034289, 2008.

Fusco, A. C. and Salby, M. L.: Interannual variations of total ozone and their relationship to variations of planetary wave activity, J. Climate, 12, 1619–1629, 1999.

Garcia, R. R., Marsh, D. R., Kinnison, D. E., Boville, B. A., and Sassi, F.: Simulation of secular trends in the middle atmosphere, 1950–2003, J. Geophys. Res., 112, D09301, doi:10.1029/2006JD007485, 2007.

Garcia-Herrera, R., Calvo, N., Garcia, R. R., and Giorgetta, M. A.: Propagation of ENSO temperature signals into the middle atmosphere: A comparison of two general circulation models and ERA-40 reanalysis data, J. Geophys. Res., 111, D06101, doi:10.1029/2005JD006061, 2006.

Garfinkel, C. I. and Hartmann, D. L.: Effects of El Nino-Southern Oscillation and the Quasi-Biennial Oscillation on polar temperatures in the stratosphere, J. Geophys. Res., 112, D19112, doi:10.1029/2007JD008481, 2007.

Hamilton, K.: An examination of observed Southern Oscillation effects in the Northern Hemisphere stratosphere, J. Atmos. Sci., 50, 3468–3473, 1993.

Hadjinicolaou, P., Pyle J. A., Chipperfield, M. P., and Kettleborough, J. A.: Effect of interannual meteorological variability on middle latitude O3, Geophys. Res. Lett., 24, 2993–2996, 1997.

Hoerling, M. P., Kumar, A., and Zhong, M.: El Niño, La Niña, and the nonlinearity of their teleconnections, J. Climate, 10, 1769–1786, 1997.

Kurokawa, J., Akiyoshi, H., Nagashima, T., Masunaga, H., Nakajima, T., Takahashi, M., and Nakane, H.: Effects of atmospheric sphericity on stratospheric chemistry and dynamics over Antarctica, J. Geophys. Res., 110, D21305, doi:10.1029/2005JD005798, 2005.

Labitzke, K. and van Loon, H.: The Southern Oscillation. Part IX: The influence of volcanic eruptions on the Southern Oscillation in the stratosphere, J. Climate, 2, 1223–1226, 1989.

Lefevre, F., Brasseur, G. P., Folkins, I., Smith, A. K., and Simon, P.: Chemistry of the 1991–1992 stratospheric winter: Three dimensional model simulations, J. Geophys. Res., 99, 8183–8195, 1994.
Manzini, E., Steil, B., Brühl, C., Giorgetta, M. A., and Krüger, K.: A new interactive chemistry-climate model: 2. Sensitivity of the middle atmosphere to ozone depletion and increase in greenhouse gases and implications for recent stratospheric cooling, J. Geophys. Res., 108(D14), 4429, doi:10.1029/2002JD002977, 2003.
Manzini, E., Giorgetta, M. A., Esch, M., Kornblueh, L., and Roeckner, E.: The influence of sea surface temperatures on the northern winter stratosphere: Ensemble simulations with the MAECHAM5 model, J. Climate, 19, 3863–3881, 2006.
McLandress, C. and Shepherd, T. G.: Simulated anthropogenic changes in the Brewer-Dobson circulation, including its extension to high latitudes, J. Climate, 22(6), 1516-1540, 2008.
Nash, J. and Edge, P. R.: Temperature changes in the stratosphere and lower mesosphere 1979–1988 inferred from TOVS radiance observations, Adv. Space Res., 9, 333–341, 1989.
Randel, W. J., Wu, F., and Stolarski, R.: Changes in column ozone correlated with the stratospheric EP Flux, J. Meteorol. Soc. Jpn., 80, 849–862, 2002.
Rozanov, E., Schraner, M., Schnadt, C., Egorova, T., Wild, M., Ohmura, A., Zubov, V., Schmutz, W., and Peter, T.: Assessment of the ozone and temperature variability during 1979–1993 with the chemistry-climate model SOCOL, Adv. Space Res., 35(8), 1375–1384, 2005.
Salby, M. L. and Callaghan, P. F.: Interannual Changes of the Stratospheric Circulation: Relationship to Ozone and Tropospheric Structure, J. Climate, 15(24), 3673–3685, 2002.
Sassi, F., Kinnison, D., Boville, B. A., Garcia, R. R., and Roble. R.: Effect of El Niño-Southern Oscillation on the dynamical, thermal, and chemical structure of the middle atmosphere, J. Geophys. Res., 109, D17108, doi:10.1029/2003JD004434, 2004.
Shibata, K., Deushi, M., Sekiyama, T. T., and Yoshimura, H.: Development of an MRI chemical transport model for the study of stratospheric chemistry, Pap. Meteorol. Geophys., 55, 75–119, 2005.
Shibata, K. and Deushi, M.: Partitioning between resolved wave forcing and unresolved gravity wave forcing to the quasi-biennial oscillation as revealed with a coupled chemistry-climate model, Geophys. Res. Lett., 32, L12820, doi:10.1029/2005GL022885, 2005.
Shiotani, M.: Annual, quasi-biennial, and El Nino-Southern Oscillation (ENSO) timescale variations in equatorial total ozone, J. Geophys. Res., 97, 7625–7633, 1992.
Spencer, R. W. and Christy, J. R.: Precision Lower Stratospheric Temperature Monitoring with

the MSU: Technique, Validation, and Results 1979–1991, J. Climate, 6(6), 1194–1204, 1993.
Steil, B., Bruehl, C., Manzini, E., Crutzen, P. J., Lelieveld, J., Rasch, P. J., Roeckner, E., and K. Krueger,: A new interactive chemistry-climate model: 1. Present-day climatology and interannual variability of the middle atmosphere using the model and 9 years of HALOE/UARS data, J. Geophys. Res., 108(D9), 4290, doi:10.1029/2002JD002971, 2003.
Steinbrecht, W., Haßler, B., Brühl, C., Dameris, M., Giorgetta, M. A., Grewe, V., Manzini, E., Matthes, S., Schnadt, C., Steil, B., and Winkler, P.: Interannual variation patterns of total ozone and lower stratospheric temperature in observations and model simulations, Atmos. Chem. Phys., 6, 349–374, 2006, http://www.atmos-chem-phys.net/6/349/2006/.
Stolarski, R. S., Douglass, A. R., Steenrod, S., and Pawson, S.: Trends in stratospheric ozone: Lessons learned from a 3d chemical transport model, J. Atmos. Sci., 63, 1028–1041, 2006.
Strauss, D. M. and Shukla, J.: Distinguishing between the SST-forced and internal variability in mid latitudes: Analysis of observations and GCM simulations, Q. J. Roy. Meteor. Soc., 126, 2323–2350, 2000.
Struthers, H., Austin, J., Kreher, K., Bodeker, G., Schofield, R., Johnston, P., Shiona, H., and Thomas, A.: Past and future simulations of NO_2 from a coupled chemistry-climate model in comparison with observations, Atmos. Chem. Phys.. 4, 2227–2239, 2004.
Tian, W. and Chipperfield, M. P.: A new coupled chemistry – climate model for the stratosphere: The importance of coupling for future O3 – climate predictions, Q. J. Roy. Meteor. Soc., 131, 281–304, 2005.
Taguchi, M. and Hartmann, D. L.: Increased occurrence of stratospheric sudden warmings during El Nino as simulated by WACCM, J. Climate, 19(3), 324–332, 2006.
Uppala, S., Kallberg, P., Hernandez, A., et al.: ERA-40: ECMWF 45-year reanalysis of the global atmosphere and surface conditions 1957–2002, ECMWF Newsletter, Vol. 101, ECMWF, Reading, United Kingdom, 2–21, 2004.
Van Loon, H. and Labitzke, K.: The Southern Oscillation. Part V: The anomalies in the lower stratosphere of the Northern Hemisphere in winter and a comparison with the quasi-biennial oscillation, Mon. Weather Rev., 115, 357–369, 1987.
Weber, M., Dhomse, S., Wittrock, F., Richter, A., Sinnhuber, B.-M., and Burrows, J. P.: Dynamical control of NH and SH winter/spring total ozone from GOME observations in 1995–2002, Geophys. Res. Lett., 30(11), 1583, doi:10.1029/2002GL016799, 2003.

Table 1. List of the models used in this work.

AMTRAC (3)	Austin et al. (2006), Austin and Wilson (2006)
CCSRNIES (3)	Akiyoshi et al. (2004), Kurokawa et al. (2005), Akiyoshi et al., (2008)
CMAM	Beagley et al. (1997), de Grandpré et al. (2000)
E39C-A	Dameris et al. (2005, 2006)
GEOSCCM	Bloom et al. (2005), Stolarski et al. (2006)
LMDZrepro	Lefevre et al. (1994)
MAECHAM4CHEM	Manzini et al. (2003), Steil et al. (2003)
MRI (5)	Shibata and Deushi (2005), Shibata et al. (2005)
SOCOL (9)	Egorova et al. (2005), Rozanov et al. (2005)
UMETRAC	Austin (2002), Austin and Butchart (2003), Struthers et al. (2004)
UMSLIMCAT	Tian and Chipperfield (2005)
WACCM (3)	Garcia et al. (2007)

ACPD
9, 12141–12170, 2009

Table 2. Warm and cold ENSO and NEUTRAL years (year index for January) for 4 WE and 6 WE.

	4 WE	6 WE
Warm	1983, 1987, 1992, 1998	1983, 1987, 1988, 1992, 1995, 1998
Cold	1985, 1989, 1996, 1999	1985, 1989, 1996, 1999
NEUTRAL	1981, 1982, 1984, 1986, 1988, 1990, 1991, 1993, 1994, 1995, 1997	1981, 1982, 1984, 1986, 1990, 1991, 1993, 1994, 1997

ACPD
9, 12141–12170, 2009

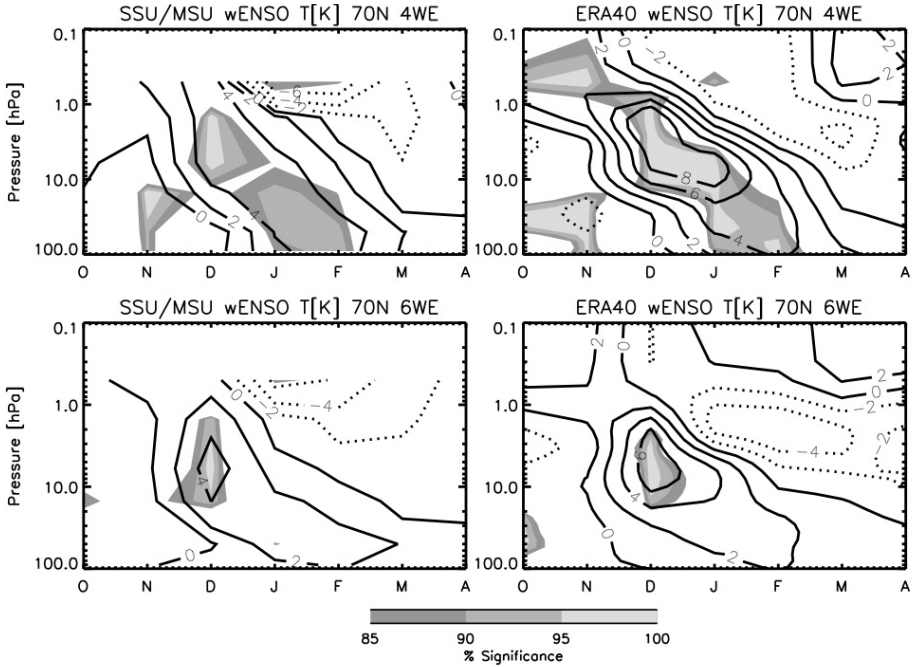

Fig. 1. Monthly zonal mean temperature ENSO anomalies (ENSO minus NEUTRAL composites) from October to April at 70° N in zonal mean temperature for (left) the MSU4/SSU satellite and (right) ERA40 reanalysis, considering (top) the 4 and (bottom) the 6 major events from 1980 to 1999. Grey shadings show the significance levels. Contour interval: 2 K, dotted lines represent negative values.

ACPD
9, 12141–12170, 2009

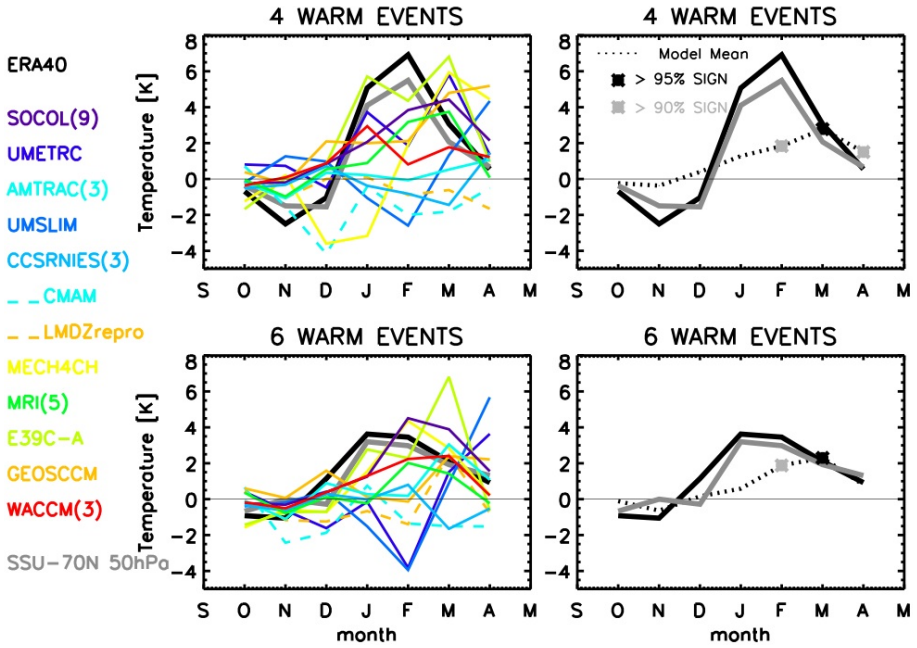

Fig. 2. (Left) Monthly zonal mean temperature ENSO anomalies from October to April, averaged over the polar cap (70° N–90° N) and the (30–70 hPa) pressure band, for each model, ERA40 (black thick line) and SSU (grey thick line). SSU anomalies are calculated at 70° N and 50 hPa. Concerning the simulations (colored lines), one curve per model is plotted, i.e. the anomaly has been averaged over the ensemble members, when available. (Right) the mean of all simulations calculated over the 30 models (dotted line) and, repeated from the left panel, ERA40 (black thick line) and SSU (grey thick line). Superimposed are significances at more than 90% (grey stars) and 95% (black stars) for the model mean. (Top) 4 ENSO events and (bottom) 6 ENSO events.

ACPD
9, 12141–12170, 2009

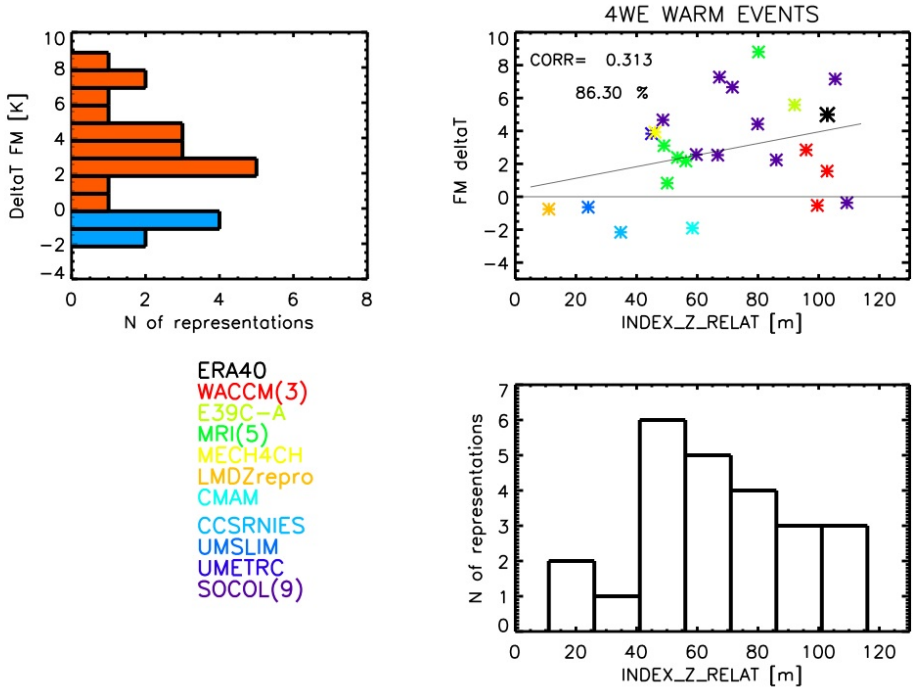

Fig. 3. (Top-left) Histogram of the temperature (K) anomaly of Fig. 2, averaged over February and March for 24 models; (top-right) scatter plot for each model and ERA40 of the temperature (K) anomaly of Fig. 2, averaged over February and March (ΔT index), versus the ΔZ index (m) at 500 hPa; superimposed the linear regression line and the correlation significance level. (Bottom-right) histogram of the ΔZ index (m) at 500 hPa for the models.

ACPD
9, 12141–12170, 2009

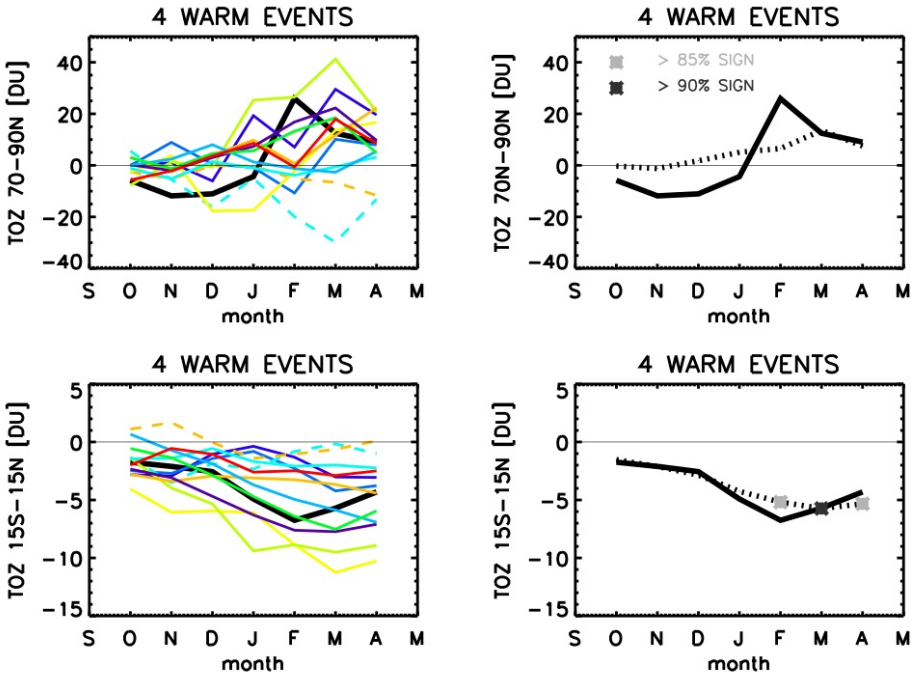

Fig. 4. Monthly zonal mean total ozone (DU) ENSO anomalies from October to April, averaged over the polar cap (70° N–90° N) (top-left) and between (15° N–15° S) (bottom-left), for each model and for NIWA. The color code for the models is the same as Fig. 2. One curve per model is plotted, i.e. the anomaly has been averaged over the ensemble members, when available. (Right) the mean of all simulations (black dots) and NIWA (black curve). Superimposed are significances at more than 90% (grey stars) and 95% (black stars) for the mean of all simulations.

ACPD
9, 12141–12170, 2009

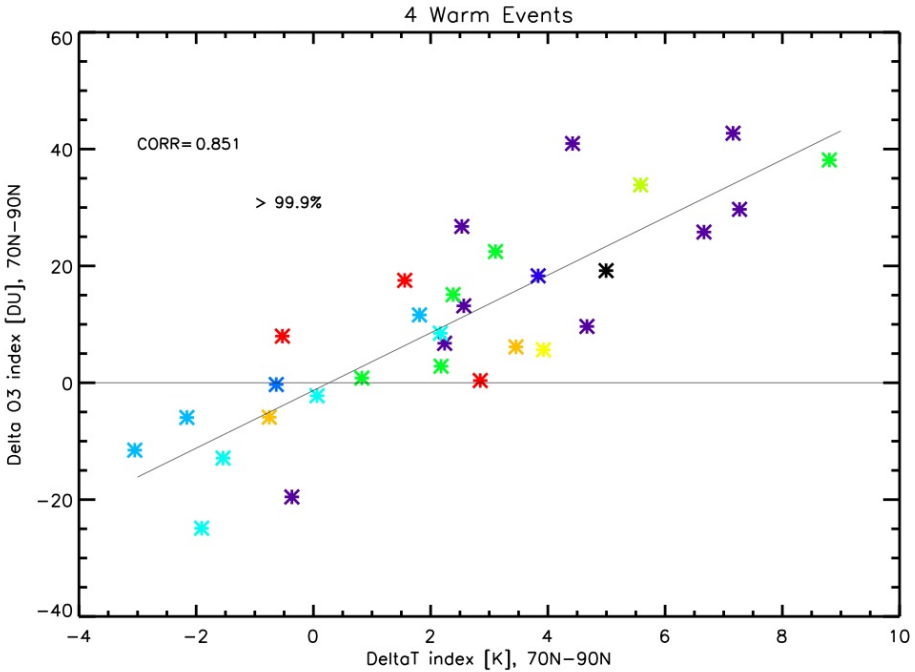

Fig. 5. Scatter plot of the ΔO3 index (total ozone ENSO anomaly, DU, of Fig. 4 top-left averaged over February and March) versus the ΔT index (temperature anomaly, K, of Fig. 2, averaged over February and March). Black star: the NIWA ΔO3 index (DU) versus the ERA40 ΔT index (K).

ACPD
9, 12141–12170, 2009

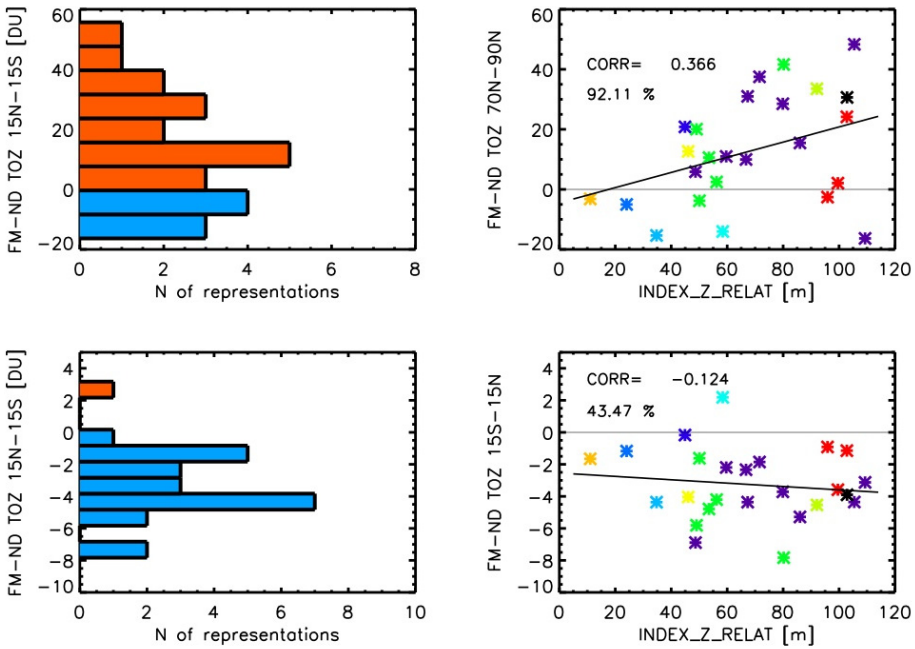

Fig. 6. (Left) Histogram of the ΔO3 (FM-ND) index (the total ozone anomaly, DU, average of February and March, minus the November–December average) for all the models at 60° N–90° N (top) and 15° N–15° S (bottom). (Right) scatter plot of the ΔO3(FM-ND) index versus the ΔZ index (m) at 60° N–90° N (top) and 15° N–15° S (bottom) for all models (in color, coded as in Fig. 3). Black stars represent the NIWA ΔO3 (FM-ND) index versus the ERA40 ΔZ index.

ACPD
9, 12141–12170, 2009